Energy 246 (2022) 123403

Contents lists available at ScienceDirect

Energy

journal homepage: www.elsevier.com/locate/energy

Time series forecasting for hourly photovoltaic power using conditional generative adversarial network and Bi-LSTM

Xiaoqiao Huang [a, b], Qiong Li [c, *], Yonghang Tai [a, b], Zaiqing Chen [b, **], Jun Liu [a], Junsheng Shi [a, b], Wuming Liu [d]

[a] School of Physics and Electronic Information, Yunnan Normal University, Kunming, Yunnan, 650500, China
[b] Yunnan Key Lab of Optic-electronic Information Technology, Kunming, Yunnan, 650500, China
[c] Solar Energy Research Institute, Yunnan Normal University, Kunming, Yunnan, 650500, China
[d] Institue of Physics, Chinese Academy of Science, Beijing, 100190, China

ARTICLE INFO

Article history:
Received 23 October 2021
Received in revised form
30 December 2021
Accepted 3 February 2022
Available online 8 February 2022

Keywords:
Bi-LSTM
Conditional generative adversarial network
Convolutional neural networks
PV power Forecasting

ABSTRACT

More and more photovoltaic (PV) power generation is incorporated into the grid. However, the intermittence and fluctuation of solar energy have brought huge challenges to the safe and stable operation of the power grid. PV power forecasting is one of the effective ways to solve the above problems, so it has become an important research topic. However, the existing research based on deep learning models mainly focuses on more complex network structures, optimization algorithms, and data decomposition. These hybrid models have encountered a development bottleneck in extracting the inherent features of PV power and related data, and a new idea and method are needed. This paper proposes a novel TSF-CGANs (time series forecasting based on CGANs, TSF-CGANs) algorithm considering conditional generative adversarial networks (CGANs) combined with convolutional neural networks (CNN) and Bi-directional long short-term memory (Bi-LSTM) for improving the accuracy of hourly PV power prediction. We design the generator in the TSF-CGANs network as a regression prediction model, which can extract the features based on historical data and random noise vector by the complex models, and finally use the Bi-LSTM model to output the predicted value. At the same time, the discriminator judges the authenticity of the generated predicted value and the actual value. In the continuous game between the generator and the discriminator, the parameters of the generator are optimized and more accurate prediction results are obtained. The performance of the proposed method is demonstrated with a real-world dataset. Compared with LSTM, recurrent neural network (RNN), back-propagation neural network (BP), support vector machine (SVM), and Persistence models, the values of five performance evaluation indicators, RMSE, MAE, nRMSE, R^2, and R, show that the proposed model has better performance in prediction accuracy. Compared with the traditional BP, the TSF-CGANs model reduced the RMSE by 32%, Compared with the Persistence, the forecast skill (FS) of TSF-CGANs is 0.4863. The results indicate that it is feasible to use the generator to realize time series prediction in the proposed TSF-CGANs network. The core idea of TSF-CGANs method is to improve the prediction accuracy of the generator through the continuous game between the generator and the discriminator, which provides a new idea for the training process of the prediction method based on deep learning.

1. Introduction

At present, an energy crisis is affecting almost every part of the world, which has led to record-high energy prices, tight supply, and power shortages. Governments all over the world have been struggling to maintain the stability of the power system. On the other hand, climate change has affected the whole world, and extreme weather conditions such as drought, heatwaves, rainstorms, floods, and landslides are becoming more and more frequent, The Intergovernmental Panel for Climate Change (IPCC) calls for carbon neutrality in the middle of the 21st century. For the

* Corresponding author.
** Corresponding author.
E-mail addresses: liqiong@ynnu.edu.cn (Q. Li), zaiqingchen@ynnu.edu.cn (Z. Chen).

https://doi.org/10.1016/j.energy.2022.123403
0360-5442/

Nomenclature

AI	artificial intelligence
ANN	artificial neural network
ARENN	asexual-reproduction evolutionary neural network
ARIMA	auto regressive integrated moving average
ARMA	autoregressive moving average
Bi-LSTM	Bi-directional long short-term memory
BP	back propagation
CGANs	conditional generative adversarial networks
CMV	cloud motion vector
CNN	convolutional neural network
ECMWF	European Centre for Medium-Range Forecasts
EEMD	ensemble empirical mode decomposition
ELM	extreme learning machine
FE	forecasting error
FS	forecast skill
GA	genetic algorithm
GANs	generative adversarial networks
GHI	global horizontal radiation
IPCC	Intergovernmental Panel for Climate Change
IRENA	International Renewable Energy Agency
LSTM	long-short term memory network
MAE	mean absolute error
nRMSE	normalized root mean square error
NWP	numerical weather prediction
PV	photovoltaic
R^2	the coefficient of determination
R	Pearson's correlation coefficient
RF	random forests
RMSE	root mean square error
RNN	recurrent neural network
SVM	support vector machine
SVR	support vector regression
TSF-CGANs	time series forecasting based on CGANs
WGANGP	Wasserstein generative adversarial networks with gradient penalty

reasons above, it has become the best choice to vigorously develop clean and renewable energy, including wind, hydropower, and solar energy, to replace traditional energy. As a kind of clean energy, PV power generation has a wide application prospect. Based on the statistics of the International Renewable Energy Agency (IRENA), the global solar PV installed capacity has reached a total of 714 GW by the end of 2020 [1]. In China, the installed PV capacity has reached 253 GW. According to IRENA's estimation, PV power generation will supply 25% of the total electricity demand by 2050. However, due to the fluctuation and intermittent of PV power, the high penetration rate of PV power will bring great difficulties to the safe, stable, and high-quality operation of the power grid system. Therefore, establishing an accurate PV power generation forecasting model is an effective way to solve this problem.

Currently, many prediction methods have been proposed for PV power forecasting. According to the classification criteria of references [2] [–] [5], the PV power forecasting model can be divided into persistence models, physical models, and statistical models. The persistence model outputs the value of a previous time as the predicted value. And the previous time can be 1 min, 1 h, 1 day, or 1week depending on the forecasting horizon.

The physical model is the method of PV power prediction only based on the main design parameters of a PV system and numerical weather prediction (NWP) and does not need any historical data [6,7]. Lorenz et al. [8] proposed a physical model for the day-ahead hourly PV power prediction based on site-specific irradiance forecasts of the European Centre for Medium-Range Forecasts (ECMWF). Wolff et al. [9] proposed the physical model combining the approach of persistence, cloud motion vector (CMV), and NWP irradiance forecasts, then, compared it with support vector regression (SVR). The results show that the prediction results of the SVR model combining all input features are similar to the proposed physical model. Mayer et al.'s research [7] provides various models to calculate physical PV power prediction models using NWP data and compares them. The conclusion shows that the beam and diffuse separation and tilted irradiance transposition models have the highest effect on the accuracy, irradiance separation and transposition modeling are the two most critical calculation steps, while the inverter model is the least important.

Statistical model uses pure mathematical equations to extract features and correlations from past input data including historical irradiance and production datasets [5]. It is a data-driven model, which requires a suitable input time horizon and high-quality input data. Traditional statistical models include regression method (RM), autoregressive moving average (ARMA) model, autoregressive integrated moving average (ARIMA) model, extreme learning machine (ELM), support vector machine (SVM), and random forests (RF) [10]. The generalized statistical model also includes various artificial intelligence (AI) models, such as deep learning models and various data-driven hybrid models. AI model can describe any complex nonlinear relationship through its good self-learning and self-organization ability, which has been widely used [11].

Some studies focused on PV power, solar irradiance, load prediction by using traditional long-short term memory network (LSTM) or bidirectional LSTM (Bi-LSTM) to extract intrinsic features of the historical data and its corresponding meteorological data and achieved good experimental results. Wang et al. [12] presented a hybrid deep learning model combining LSTM and convolutional neural network (CNN), in which the temporal features of the data are extracted by LSTM, and then the spatial features are extracted by the CNN. The results indicate that the prediction accuracy of the proposed LSTM-CNN model is better than the single model. Zhen et al. [13] proposed the hybrid model which combines Bi-LSTM and genetic algorithm (GA) to enhance the forecasting accuracy. Abdel-Abdel-Basset et al. [14] introduced a novel data-driven PV-Net to forecast short-term PV power, which redesigned the gates of GRU using convolutional layers. Results showed that the PV-Net improves feature extraction from PV time series and has high accuracy.

Recently, a new generation model, generative adversarial networks (GANs), has been developed to overcome the problem of sample shortage, which has been applied to image processing [15], computer vision [16], speech and natural language processing [17], and financial time-series modeling [18], and so on. Due to the powerful modeling ability of GANs through continuous self-learning, it can generate new data with similar characteristics to the original data [19]. In the field of energy prediction, some scholars have done some research using GANs.

Hu et al. [20] used improved GANs to extract the temporal and spatial characteristics of wind and photovoltaic power generation, which improve the efficiency of power generation planning. To improve the accuracy of PV power forecasting, Wang et al. [19]. proposed the weather classification model based on Wasserstein

generative adversarial networks with gradient penalty (WGANGP) and CNN. The results show that WGANGP can generate new samples by obtaining the internal characteristics of the original series, rather than simply memorizing the training data [19]. Bendaoud et al. [21] introduced the application of GAN to forecast the short-term load and presents a conditional GAN (CGAN) to predict a daily load using maximum and minimum temperature, day of the week, and month. Yin et al. [11] presented a new method for short-term wind power forecasting based on asexual-reproduction evolutionary neural network (ARENN), WGANGP, and ensemble empirical mode decomposition (EEMD). In their research, different kinds of GANs were used to generate approximate real data to expand the training data set. Chen et al. [22] proposed a GAN constructed with two interconnected deep neural networks for the renewable scenario generation. Zhou et al. [23] and Yuan et al. [24] used GAN and PG-GAN to forecast wind power, respectively.

However, as we all know, GANs are hard to train, and often suffer from mode collapse and the discriminator winning the contest [25]. Meanwhile, the traditional GANs or CGANS network is mainly used to generate artificial data with similar distribution characteristics as the training sample, to expand the training set and enhance the generalization performance [19,23,26–29]. Koochali et al. [30] introduced the probabilistic forecasting method with CGANs, named ForGAN. However, the method of time series predicting based on point forecasting has not been reported so far.

In this paper, a point forecasting model named TSF-CGANs is proposed based CGANs, CNN, and Bi-LSTM for hourly PV power forecasting. In our method, the noise vector and the conditional matrix are integrated into the generator of TSF-CGANs for semi-supervised regression learning, which can extract inherent nonlinear and dynamic features from the historical data of the PV power and corresponding meteorological data, and improve the accuracy of PV power prediction. The main contributions of this paper can be summarized as follows:

- We propose TSF-CGANs, a novel approach to employ CGANs for forecasting hourly PV power value, which is the first attempt in this field and is also used for other time series forecasting.
- The proposed TSF-CGANs network combining CGANs, CNN, and Bi-LSMT, not only has the characteristics of adversarial learning with the common CGANs but also has the characteristics and structure of regression models. Therefore, it can improve the predictive performance of the generator in continuous generative adversarial learning.
- The proposed condition matrix contains historical PV power, time information, and meteorological data information. TSF-CGANs model extracts the internal characteristic information from condition information and noise vector to predict the time-varying power output of PV power generation.
- The proposed TSF-CGANs approach is validated by the case study based on the real PV power dataset from Alice Springs, Australia.

2. Methodology

2.1. Generative adversarial network (GAN)

Generative adversarial network (GAN) is a generation model proposed by Goodfellow [31], which is a method of unsupervised learning on complex distributions. There are two models, named discriminator (D) and generator (G), in GAN, and which can be various nonlinear mapping functions, such as machine learning model and deep neural network. The main task of the discriminator is to determine whether a sample is false or true. The main objective of the generator is to deceive the discriminator by generating samples highly resembling the original data. The discriminator outputs the probability that a given sample is a real sample. The higher the probability value, the closer the sample is to the real sample and vice versa.

In the game competition, both models D and G continue to evolve until they reach the Nash equilibria, that is, the data generated by model G is similar to the original data [32], indicating that the GAN has completed training. At this time, the probability of the discriminator output is 0.5. The basic idea of GAN is the minimax of the game between the generator and the discriminator.

The structure diagram of GAN is shown in Fig. 1, and its mathematical description is as follows [28]:

x represents the real data samples, and is data distribution for real samples, z represents random noise variables, G(z) represents the sample generated by G which can obey the distribution $P_{data}(x)$ of the real sample, $P_z(z)$ represents the data distribution over noise input z, $\mathbb{E}$ denotes expectation.

For discriminator (D), on the one hand, D is expected to have a higher output probability of $D(x)$ for the real sample; on the other hand, D is expected to have a lower output probability of $D(G(z))$ for the generated sample. The loss function can be defined in Eq. (1):

$$L_D = -\mathbb{E}_{x\sim P_{data}(x)}[logD(x)] - \mathbb{E}_{z\sim P_z(z)}[\log(1-D(G(z)))] \quad (1)$$

For generator (G), a series of noise sampled from $P_z(z)$ is used as the input, G captures the true data distribution by continuously updating parameters until the generated samples are as real as possible. During the iterative process, maximize $D(G(z))$ is the goal of G. The loss function can be defined in Eq. (2):

$$L_G = \mathbb{E}_{z\sim P_z(z)}[\log(1-D(G(z)))] \quad (2)$$

For GAN, the whole loss function is shown in Eq. (3).

$$\min_G \max_D L(D,G) = \mathbb{E}_{x\sim p_{date(x)}}[logD(x)] + \mathbb{E}_{z\sim P_z(z)}[\log(1-D(G(z)))] \quad (3)$$

Conditional generative adversarial networks (CGANs) are an improvement of the basic GAN framework, which can generate synthetic data more targeted by adding some additional condition information y to the generator and the discriminator. At this time, z becomes $(z|y)$, and x becomes $(x|y)$ in Equations (1)–(3). The additional condition information here can be any type of information that helps capture the features in data distribution of x, such as class labels in image recognition, meteorological and solar module array feature data in PV power prediction, or data from other modalities [33]. The objective function $L(D,G)$ can be written as followed:

$$\min_G \max_D L(D,G) = \mathbb{E}_{x\sim p_{date(x)}}[logD(x|y)] + \mathbb{E}_{z\sim p_{z(z)}}[log(1-D(G(z|y)))] \quad (4)$$

The structure diagram of CGAN is shown in Fig. 2.

2.2. Long short term memory (LSTM) and bidirectional LSTM (Bi-LSTM)

To solve the gradient vanishing and explosion problem of RNN, Hochreiter and Schmidhuber proposed Long short-term memory (LSTM) [34]. LSTM has obvious advantages in time series forecasting because it effectively solves the problem of long-term and short-term dependencies, which is widely used in the fields of irradiance forecasting and photovoltaic power forecasting [35–41].

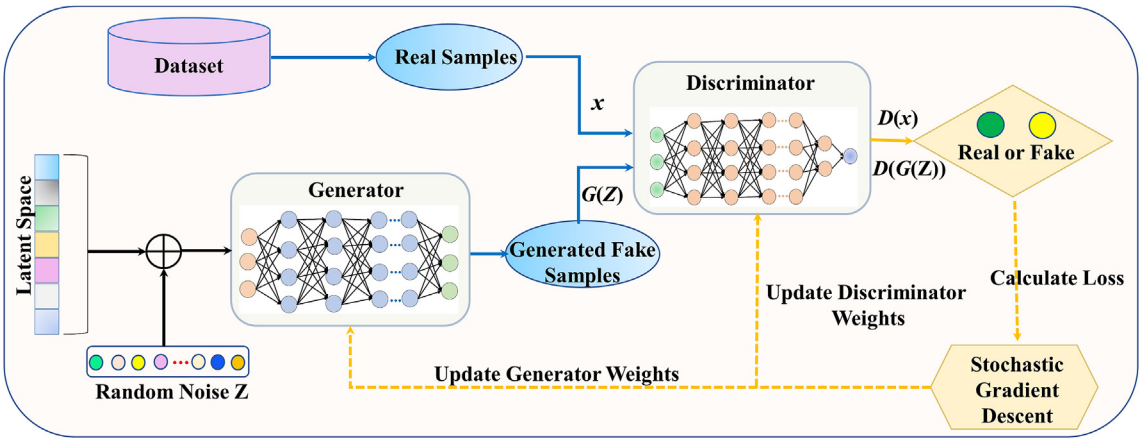

Fig. 1. Architecture of the GAN.

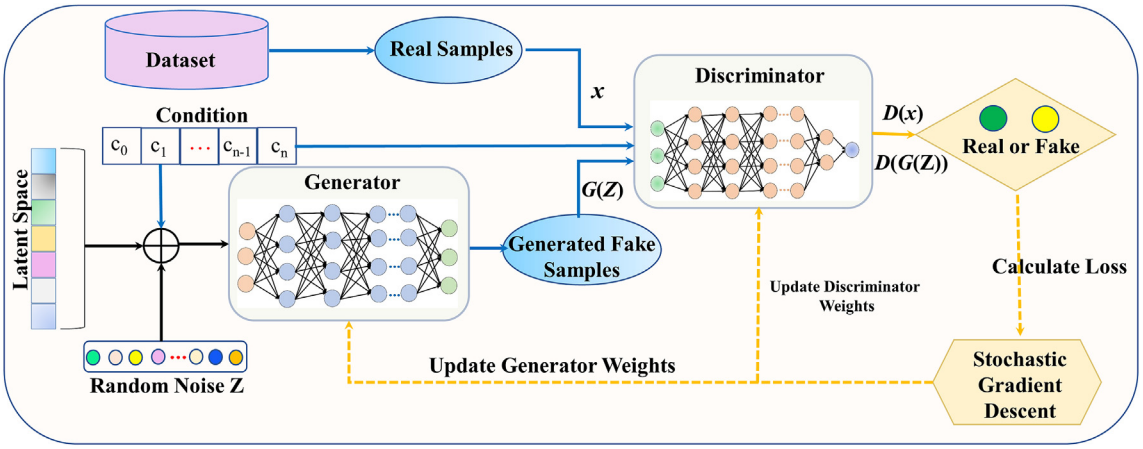

Fig. 2. Architecture of the CGAN

There are three gate controls: input gate (i_t), output gate (o_t), and forget gate (f_t) in LSTM cell.

The structure of the LSTM unit is shown in Fig. 3(a), and the main calculation process is described as follows:

$$i_t = \sigma(W_{ix}x_t + W_{im}m_{t-1} + W_{ic}c_{t-1} + b_i) \tag{5}$$

$$f_t = \sigma\left(W_{fx}x_t + W_{fm}m_{t-1} + W_{fc}c_{t-1} + b_f\right) \tag{6}$$

$$c_t = f_t \odot c_{t-1} + i_t \odot g(W_{cx}x_t + W_{cm}m_{t-1} + b_c) \tag{7}$$

$$o_t = \sigma(W_{ox}x_t + W_{om}m_{t-1} + W_{oc}c_{t-1} + b_o) \tag{8}$$

$$m_t = o_t \odot h(c_t) \tag{9}$$

$$y_t = \varphi(W_{ym}m_t + b_y) \tag{10}$$

where c_t represent the memory cell, w and b are the weight matrices and the bias vectors, respectively, x_t denotes the input data at a present time step t, σ is the sigmoid function, and φ is the output activation function.

The bidirectional LSTM (Bi-LSTM) model is shown in Fig. 3(b), which includes a forward LSTM layer and a backward LSTM layer. $\overrightarrow{h}_t$ and $\overleftarrow{h}_t$ is used to denote the LSTM hidden vector of the forward LSTM layer and backward LSTM layer at time t, respectively. As shown in Fig. 3(b), $\overrightarrow{h}_t$ and $\overleftarrow{h}_t$ are independent of each other and are only related to their respective LSTM layers. The corresponding output of Bi-LSTM (y_t) is obtained by the weighted connection of these two hidden layers. The process can be described as:

$$\overrightarrow{h}_t = LSTM\left(x_t, \overrightarrow{h}_{t-1}\right) \tag{11}$$

$$\overleftarrow{h}_t = LSTM\left(x_t, \overleftarrow{h}_{t+1}\right) \tag{12}$$

$$y_t = \delta\left(W_{\overrightarrow{h}_y}\overrightarrow{h}_t + W_{\overleftarrow{h}_y}\overleftarrow{h}_t + b_y\right) \tag{13}$$

where $LSTM(\cdot)$ represents LSTM network, $W_{\overrightarrow{h}_y}$ and $W_{\overleftarrow{h}_y}$ represent the weight of the forward and backward LSTM layer at time t, respectively. b_y denotes the bias of the output layer, $\delta(\cdot)$ represents the activation function.

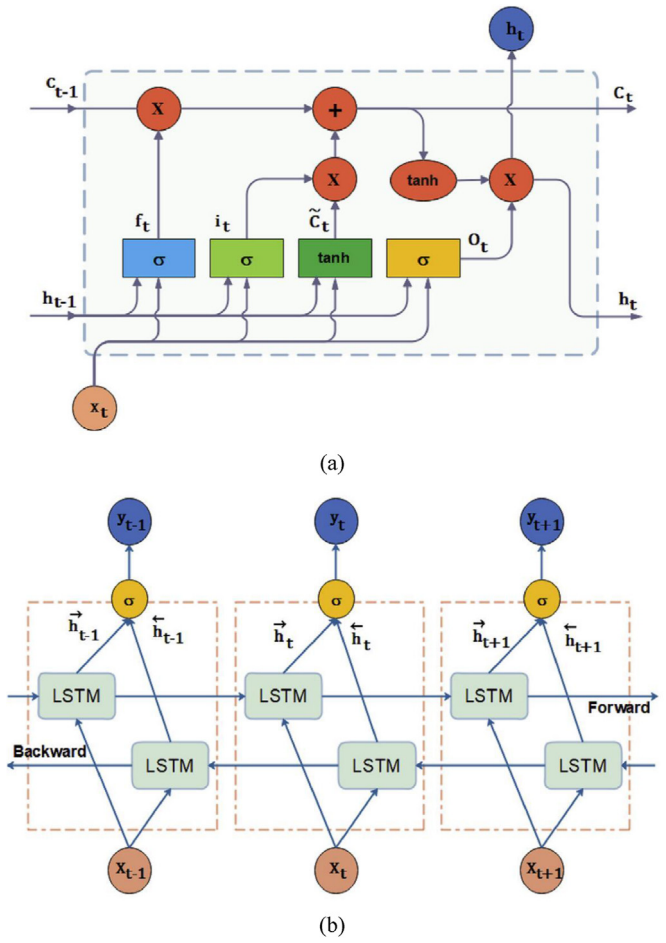

Fig. 3. Architecture of (a) LSTM cell (b) Bi-directional LSTM [40].

2.3. The proposed TSF-CGANs model

2.3.1. Problem statement

We model the problem of PV power prediction as a regression problem:

$$Y = f(X) \tag{14}$$

where X indicates the input of historical data, including active PV power, relative humidity, temperature, global horizontal radiation (GHI), hour, and so on, Y represents the predicted value, $f(\cdot)$ represents various regression functions, such as ARIMA, various CNN, RNN, LSTM, and so on. To improve the performance of the model, we considered adding Gaussian noise to the latent variables, and at the same time, using historical data as the conditional input. So the expression becomes as follows:

$$Y = G(z, X) \tag{15}$$

where z represents the noise in the latent, $G(\cdot)$ represents the generator of the proposed TSF-CGANs model, X also represents historical data, here as the conditioned matrix of TSF-CGANs.

It is generally believed that the input to the model is a time series. So the input sequence is described as:

$$\mathrm{X} = (X_{t-23}, X_{t-22}, X_{t-21}, \cdots, X_{t-1}, X_t) \tag{16}$$

where the subscript t represents any time, for any X_t in the above formula, it is composed of multiple parameter variables at time t, described as follows:

$$X_t = (Power_t, \mathrm{GHI}_t, \mathrm{Temperature}_t, \cdots, Hour_t) \tag{17}$$

2.3.2. The framework description of the proposed prediction model

The proposed prediction structure combining CNN, Bi-LSTM, and CGANS can be seen in Fig. 4. Compared with the traditional CGANS, which is mainly used to generate artificial data with similar distribution to the real data, this paper proposes a novel structure of CGANS named TSF-CGANS to predict the data. To utilize the advantages of the Bi-LSTM network's time series prediction, the Bi-LSTM network is used in both generator and discriminator for making the generated data have the characteristics of time series. Meanwhile, from related research, we found that historical data plays an important role in statistical forecasts based on AI. Therefore, we have selected PV power history data and related meteorological data as the input of the conditioned matrix of TSF-CGANS. The detailed structure of the generator and discriminator in the TSF-CGANs network can be seen in Fig. 5.

Firstly, use the generator to generate forecast data. The specific process can be explained as (1) Taking noise matrix and condition matrix (including historical PV power, historical weather data) as the input of the model; (2) Acquiring a high-dimensional feature map of the input noise matrix by the convolution and pooling; (3) Multiplying the feature matrix and condition matrix; (4) Extracting the feature of time series based on Bi-LSTM; (5) Forecasting the PV power at next time by the output of fully connected layer.

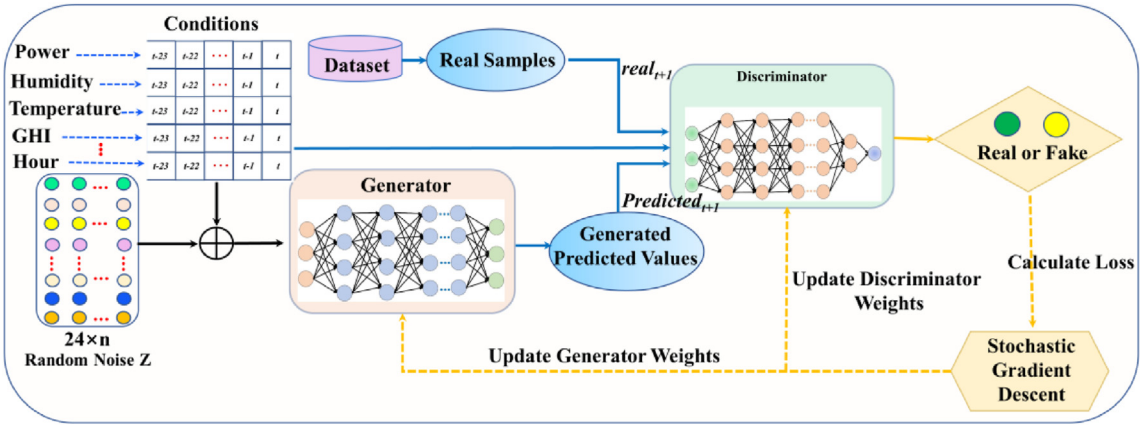

Fig. 4. Overview of proposed TSF-CGANs architecture. The condition matrix is used in both generator and discriminator.

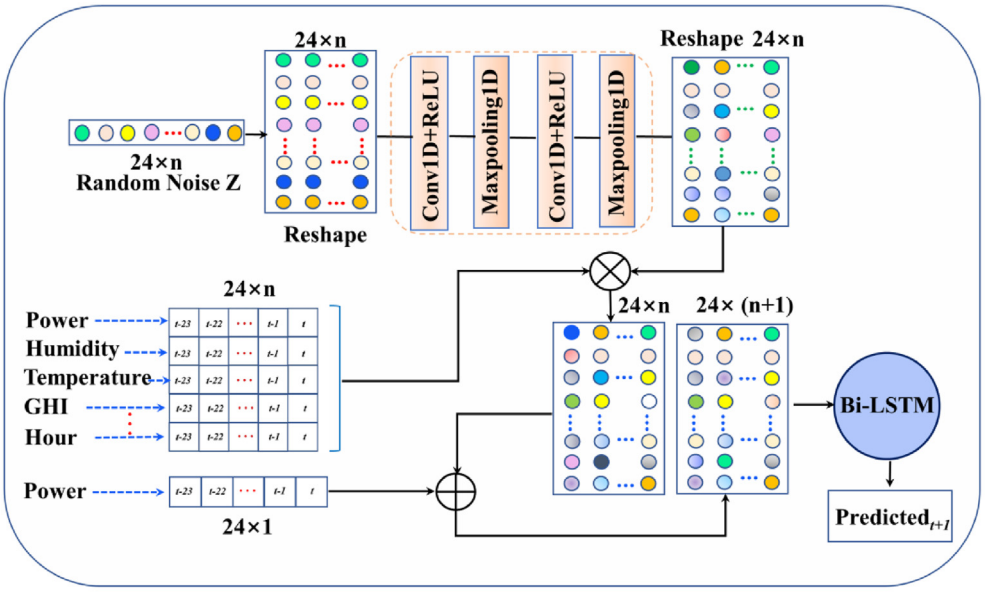

(a)

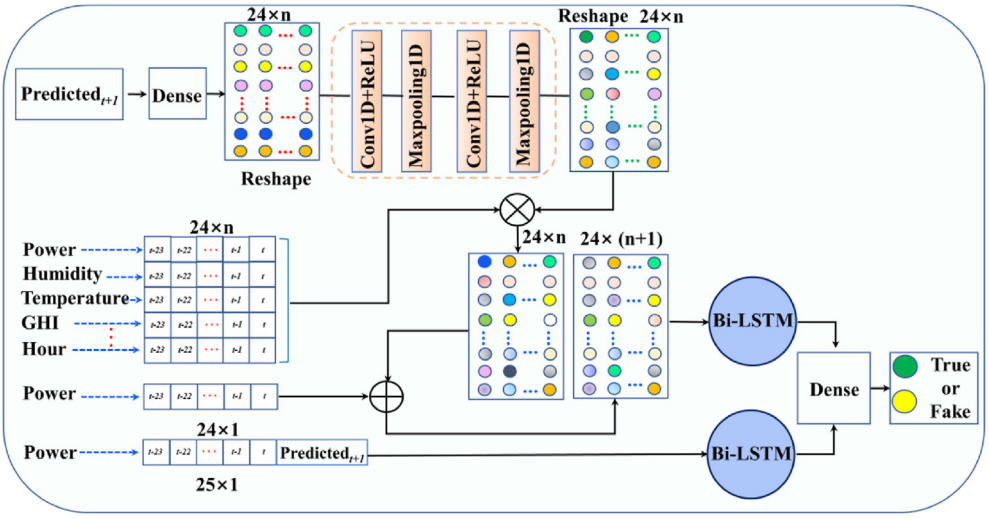

(b)

Fig. 5. (a): The detailed structure of the generator in the TSF-CGANs network. The generator generates predicted PV power values using the conditioned matrix and the noise. (b): The detailed structure of the discriminator in the TSF-CGANs network. The discriminator discriminates whether the predicted value is true or false based on the conditioned matrix and the predicted value.

Specifically, the three inputs are designed in the generator and are represented as $Input_{1G}$ (Random noise), $Input_{2G}$ (condition matrix_all historical data), and $Input_{3G}$ (condition vector_PV power historical data), respectively. The main calculation process is described as follows:

$$H_{g1} = con1D(Input_{1G}) \tag{18}$$

$$H_{g2} = Multiply(Input_{2G}, H_{g1}) \tag{19}$$

$$H_{g3} = Concatenate(Input_{3G}, H_{g2}) \tag{20}$$

$$H_{g4} = BiLSTM(H_{g3}) \tag{21}$$

$$Output_g = Dense(H_{g4}) \tag{22}$$

where $con1D(\cdot)$ represents one-dimensional CNN, $Multiply(\cdot)$ represents multiplying operator in Python, $Concatenate(\cdot)$ represents concatenating two different matrices together, $BiLSTM(\cdot)$ represents Bi-LSTM network, $Dense(\cdot)$ represents the regular deeply connected neural network layer.

Secondly, use the discriminator network to discriminate the generated predicted value. The specific process can be explained as (1) Taking the predicted value generated by the generator and condition matrix (including historical PV power, historical weather data) as the input of the model; (2) Expanding the predicted value

with a fully connected layer; (3) Acquiring a high-dimensional feature map of the augmentation predicted value by the convolution and pooling; (4) Multiplying the feature matrix and condition matrix; (5) Extracting the feature of time series based on Bi-LSTM for different feature matrix; (6) Determining whether the predicted value is true or false by the output of fully connected layer. Specifically, there are also three inputs in the discriminator, represented as $Input_{1D}$ (the generated predicted value), $Input_{2D}$ (condition matrix_all historical data), and $Input_{3D}$ (condition vector_PV power historical data). The main calculation process is described as follows:

$$H_{d1} = Dense(Input_{1D}) \tag{23}$$

$$H_{d2} = con1D(H_{d1}) \tag{24}$$

$$H_{d3} = Multiply(Input_{2D}, H_{d2}) \tag{25}$$

$$H_{d4} = BiLSTM(H_{d3}) \tag{26}$$

$$H_{d5} = Concatenate(Input_{3D}, Input_{1D}) \tag{27}$$

$$H_{d6} = BiLSTM(H_{d5}) \tag{28}$$

$$Output_d = Dense(Concatenate(Dense(H_{d4}), Dense(H_{d6}))) \tag{29}$$

where the meaning of the variables is the same as above.

Finally, the generator and the discriminator are trained iteratively, and the two continue to play games, which has achieved the goal of the predicted data generated by the generator as close to the actual data as possible.

The complete TSF-CGANs training process is also concluded in Algorithm 1. Analyzing the algorithm, we can find that when the predicted value generated by the generator is closer to the true value, the discriminator is easier to find its optimal parameters. Meanwhile, the parameters of the generator will update according to the judgment of the authenticity of the prediction result by the discriminator. The generator and discriminator of TSF-CGAN are optimized alternately to achieve Nash equilibrium based on min-max optimization. Finally, the result of the generator in TSF-CGANs is extracted as the predicted output of the hourly PV power.

Algorithm 1
Time series forecasting model-conditional generative adversarial network (TSF-CGANs).

Require: the batch size m, Adam (stochastic gradient algorithm) hyper-parameters $\{\alpha, \beta_1, \beta_2\}$.
Require: Initialize the parameter of the generator θ_G and discriminator θ_D.
1: **for** the number of training iterations **do**
2: Sample a batch of $\{x^{(i)}\}_{i=1}^{m} \sim P_{data}$ a (training data, as the conditioned matrix of the TSF-CGANs) and $\{z^{(i)}\}_{i=1}^{m} \sim P_z$ (noise samples)
3: Using Equation 18–22 to obtain $\{G(x^{(i)}, z^{(i)})\}_{i=1}^{m}$ (generator)
4: Using Equation 23–29 to obtain $\{D(G(x^{(i)}, z^{(i)}), x^{(i)})\}_{i=1}^{m}$ (discriminator)
5: Computer the loss function L_G of the generator based on Equation (1).
6: Computer the loss function L_D of the discriminator based on Equation (2).
7: Computer the loss function $L_{D,G}$ of the TSF-CGANs based on Equation (3).
8: $\nabla\theta_G \leftarrow Adam(\theta_D, \{G(x^{(i)}, z^{(i)})\}_{i=1}^{m}, \alpha, \beta_1, \beta_2)$
9: Update $\theta_G \leftarrow \theta_G - \eta_G \nabla\theta_G$.
10: $\nabla\theta_D \leftarrow Adam(\theta_D, \{D(G(x^{(i)}, z^{(i)}), x^{(i)})\}_{i=1}^{m}, \alpha, \beta_1, \beta_2)$
11: Update $\theta_D \leftarrow \theta_D - \eta_D \nabla\theta_D$.
12: **end for**
13: Predict the PV power using the trained generator

2.3.3. The structure of the input data

In the three stages of training, verification, and testing, the features of the historical time series of the past 24 h include active power, relative humidity, temperature, global horizontal radiation, and, hours. These features correspond to relevant parameters at time $t,\ t-1, \cdots,\ t-23$, are fed to the proposed network as conditional matrix inputs. The actual and predicted PV power at the next time step $(t+1)$ is fed as input to the discriminator model, as well as the conditioned matrix. Note that the interval of t in here is 1 h. For the next sample, the input values can be obtained by sliding the window on the time series at an interval of 1 h, for example, the values at $t-1,\ t-2, \cdots,\ t-24$ as inputs, the values at t as output. This can be illustrated in Fig. 6.

2.4. Performance evaluation index

The general evaluation indexes of the time series prediction model are as follows:

Mean absolute error (MAE)

$$\mathrm{MAE} = \frac{1}{N}\sum_{i=1}^{N}|P_i - \widehat{P}_i| \tag{30}$$

Root mean square error (RMSE)

$$RMSE = \sqrt{\frac{1}{N}\sum_{i=1}^{N}(\widehat{P}_i - P_i)^2} \tag{31}$$

Normalized root mean square error (nRMSE)

$$nRMSE = \frac{RMSE}{\overline{P}} \times 100\% \tag{32}$$

The coefficient of determination (R^2)

$$R^2 = 1 - \frac{\sum_{i=1}^{N}(\widehat{P}_i - \overline{P})^2}{\sum_{i=1}^{N}(P_i - \overline{P})^2} \tag{33}$$

Pearson's correlation coefficient (R)

$$\mathrm{R} = \frac{\sum_{i=1}^{N}(P_i - \overline{P}_i)(\widehat{P}_i - \overline{\widehat{P}})}{\sqrt{\sum_{i=1}^{N}(P_i - \overline{P})^2}\sqrt{\sum_{i=1}^{N}(\widehat{P}_i - \overline{\widehat{P}})^2}} \tag{34}$$

where $\widehat{P}_i$ represents the forecasted PV power values, P_i represents the true values and N is the number of samples, $\overline{P}$ represents the average of true values, $\overline{\widehat{P}}$ represents the average forecasted value.

3. Case study and discussions

3.1. Data source and experimental setup

In this paper, the 1B DKASC's PV system data (the Desert Knowledge Australia Solar Centre, DKASC) (Trina, 23.4 kW, mono-Si, Dual, 2009), in Alice Springs [42], was used in the following case research. The five years (2014–2018) data was selected for this case, and the data sampling interval is 5 min. In this paper, we consider hourly PV power, and 5-min data is transformed to hourly data by an averaging method. So, there are a total of 8760 sets of data in a year. The data from 2014 to 2017 was set as the training dataset. The data in 2018 was set as the test dataset.

We select the relatively complete parameters from the downloaded data, including active power (P, kW), relative humidity (RH, %), weather temperature (WT, °C), global horizontal radiation (GHI,

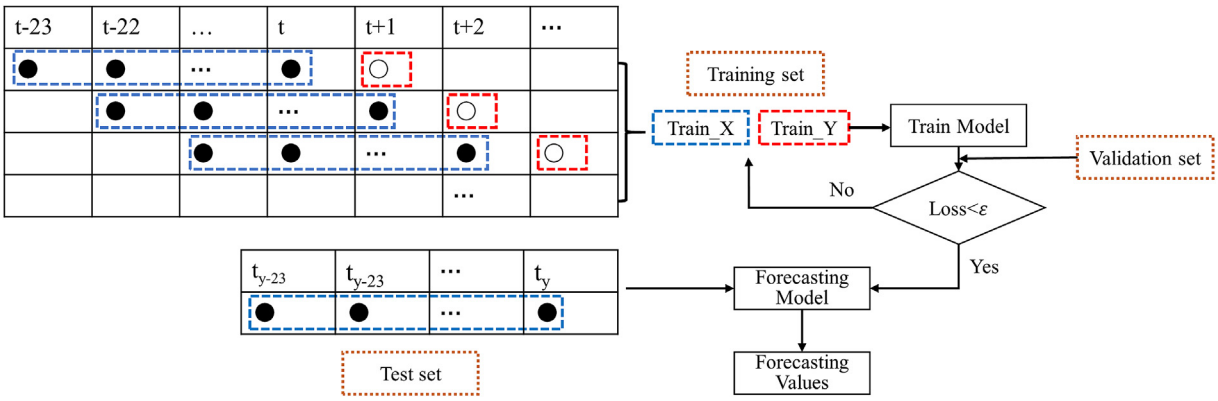

Fig. 6. Description of variables for PV power forecasting.

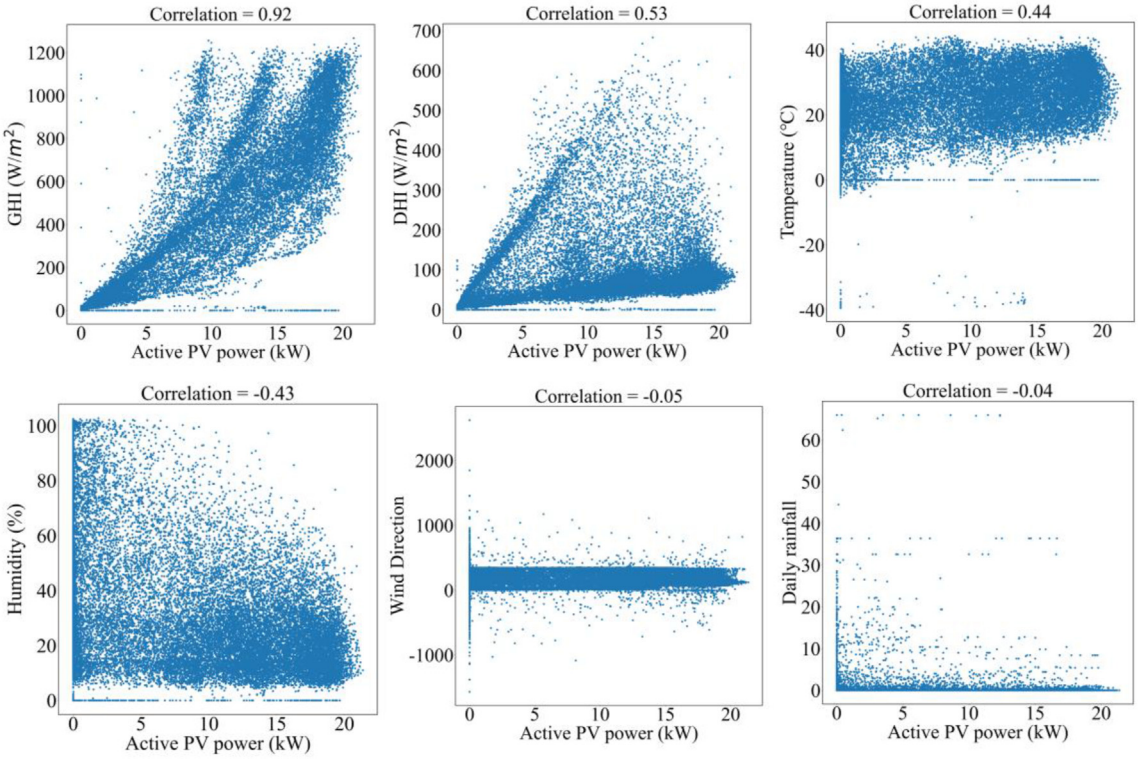

Fig. 7. Pearson correlation coefficients between PV power and other parameters.

W/m^2), diffuse horizontal radiation (DHI, W/m^2), wind direction (WR), daily rainfall (DR), time (T), etc. Among them, the missing data is filled with adjacent values.

To select the most relevant feature of PV power as input, the Pearson correlation (R) between PV power (P) and meteorological parameters (RH, WT, GHI, DHI, WR, DR, T) was calculated. Fig. 7 shows the results of Pearson correlation coefficients for these variables. As can be seen from the figure, GHI and PV power have the highest correlation. This is very obvious because the PV power is mainly determined by the global horizontal radiation arrived at the PV panel, of course, DHI also plays an important role. Wind direction and rainfall have almost no correlation with PV power. Theoretically speaking, rainfall should affect the output of PV power, but because the data set we choose is from the arid climate of a tropical desert, the rainfall is very small, and the fluctuation of PV power is more caused by cloud cover. In this paper, we discarded the wind direction and rainfall.

All experiments were implemented based on Python 3.6.1 with Tensorflow 1.13. The hardware platform is a high-performance Lenovo ThinkStation computer with Intel (R)Core(TM) i7-8700 CPU @3.20 GHz, 16.00 GB RAM, and NVIDIA GeForce GTX 1080 GPU.

3.2. Model design and related parameter selection

To accelerate the convergence of the neural network, referring to the general method, firstly, the PV power other data are normalized to the range of [0,1] through the MinMaxScaler function. (After the model training process is completed, the output data is then denormalized to the original range). The dimension of the input uniform noise of the generator depends on the dimension

of the input condition matrix, and its range is [0, 1]. In the TSF-CGANs proposed here, 24 × 6 dimensions are selected. The optimizer of the generator and discriminator is Adam in this model. Except for the sigmoid in the output layer, all other layers use ReLU activation. The learning rate is 0.0001, the epoch is set to 10,000, and the batch size is 500. The specific details of each network are shown in Table 1.

3.3. Results

The prediction results of the proposed TSF-CGANs model are shown in Fig. 8 and Table 2. Fig. 8 shows a scatter plot of the measured data and the predicted results calculated by TSF-CGANs models. If the predicted value is equal to the actual value, then all points should be on one line (y = x). The red solid line is the best linear fit of the scattered data, and its slope is 1.00678, which is very close to k = 1, indicating that the predicted value and the actual value have good linearity. Table 2 shows the evaluation index of six different PV power forecasting models. From the last row in Table 2, we can see that the RMSE of the proposed model is 0.964, MAE is 0.483, nRMSE is 24.16%, R^2 is 0.9621, and R is 0.9823.

Fig. 9 shows the average value and standard deviation of the PV power at different periods of the day in a one-year test sample. The solid line in the middle represents the average, and the upper and lower shading represents the standard deviation. It can be seen from Fig. 9 that the average value at noon is large, indicating that the irradiance is strong and the PV power output is large, and the corresponding standard deviation at this time is also large, which is consistent with the statistical rules. It can be seen from the mixed distribution map (right) that the predicted value (red) is slightly larger than the actual value (green), but the overall coincidence (shadow color) is better. This also shows that the fact of adding time (hour) in the conditioned matrix of the CGAN's has proven to be

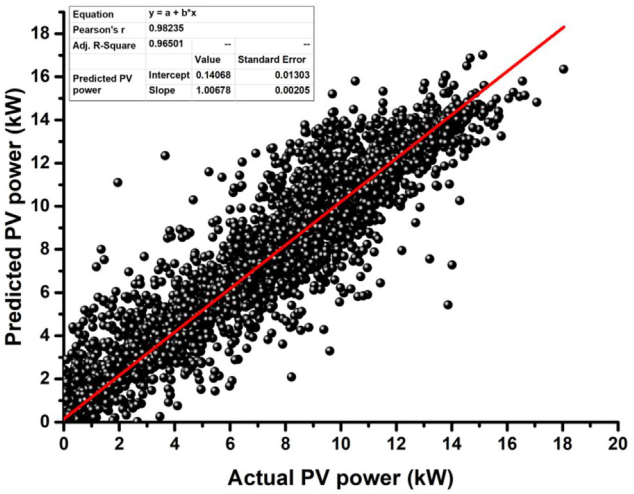

Fig. 8. Scatter plot of predicted and actual values.

Table 1
The architectures of the generator and discriminator networks.

Generator networks G
Input_1(InputLayer): Noise z, (None, 144)
Layer 1: Reshape to (None, 24, 6)
Layer 2: Conv1D, (filters = 32, kernel_size = 2, padding = 'same'), (None, 24, 32)
Layer 3: MaxPooling1D, (pool_size = 2), (None, 12, 32)
Layer 4: Conv1D, (filters = 64, kernel_size = 2, padding = 'same'), (None, 12, 64)
Layer 5: MaxPooling1D, (pool_size = 2), (None, 6, 64)
Layer 6: Flatten, (None, 384)
Layer 7: Dense, (None, 144)
Layer 8: Reshape, (None, 24, 6)
Layer 9: **Input_2** (InputLayer), (None, 24, 6)
Layer 10: Multiply, (None, 24, 6)
Layer 11: **Input_3** (InputLayer), (None, 24), Reshape, (None, 24, 1)
Layer 12: Concatenate, (None, 24, 7)
Layer 13: Bidirectional LSTM, (LSTM(24)), (None, 48)
Layer 14: Dense, output, (None, 1)
Output: The predicted PV power at t+1
Discriminator networks D
Input_1(InputLayer): The predicted PV power at t+1, (None, 1)
Layer 1: Dense, (144), (None, 144)
Layer 2: Reshape, (None, 24, 6)
Layer 3: Conv1D, (filters = 32, kernel_size = 2, padding = 'same'), (None, 24, 32)
Layer 4: MaxPooling1D, (pool_size = 2), (None, 12, 32)
Layer 5: Conv1D, (filters = 64, kernel_size = 2, padding = 'same'), (None, 12, 64)
Layer 6: MaxPooling1D, (pool_size = 2), (None, 6, 64)
Layer 7: Flatten, (None, 384)
Layer 8: Dense, (None, 144)
Layer 9: Reshape, (None, 24, 6)
Layer 10: **Input_2** (InputLayer), (None, 24, 6)
Layer 11: Multiply, (None, 24, 6)
Layer 13: Bidirectional LSTM, (LSTM(24)), (None, 48)
Layer 14: **Input_3** (InputLayer), (None, 24), Reshape, (None, 24, 1)
Layer 15: Concatenate, (Input_3, Input_1), (None, 25), Reshape, (None, 25, 1)
Layer 16: Bidirectional LSTM, (LSTM(24)), (None, 48)
Layer 17: Dense, 12, (None, 12), 24, (None, 24)
Layer 18: Dense, activation = 'sigmoid', output, (None, 1)
Output: Real or Fake

Note: In Generator networks, G, the input of multiplication operation in the "Layer 10" is the Input_2 in the "Layer 9" and the output of the "Layer 8". The input of concatenate operation in the "Layer 12" is the Input_3 in the "Layer 11" and the output of the "Layer 10".

Table 2
Comparison of prediction performance of six models.

	RMSE (kW)	MAE (kW)	nRMSE (%)	R^2	R
Persistence	1.983	1.075	49.68	0.8395	0.9198
BP	1.420	0.731	35.57	0.9178	0.9665
SVM	1.277	0.957	31.99	0.9335	0.9666
RNN	1.008	0.574	25.26	0.9585	0.9802
LSTM	0.993	0.517	24.87	0.9598	0.9801
Proposed TSF-CGANs	0.964	0.483	24.16	0.9621	0.9823

essential for enhancing the model's behavior at a specific time and adapting to the time changes of PV power prediction.

To analyze the hour-to-hour PV power prediction performance, forecasting error (FE) is used in this paper, which describes the difference between hourly actual PV power (P_i) and hourly forecasted value ($\widehat{P}_i$). The mathematical description of FE is FE $= \widehat{P}_i - P_i$. The results are shown in Fig. 10. The mean value and the standard deviation (σ) of FE, and the number of datum points which the error is during $(0 \sim 1)\sigma$, $(1 \sim 2)\sigma$, $(2 \sim 3)\sigma$ and $(3+)\sigma$ are also described in Fig. 10(a). As it can be seen in Fig. 10(a), the standard deviation of the TSF-CGANs model's FE is 0.9496, datum point (75.5%) in $<1\sigma$ range is 7218 which accounts for 82.4% of all data. As seen in Fig. 10(b), most errors are distributed in places less than 0 but very close to 0, meanwhile, the error is negative, indicating that most of the predictions are very close to the true value and slightly smaller than the true value. When the FE is slightly larger, the positive number is slightly more than the negative number, which means that for the predicted value with a large error, the predicted value is often larger than the actual value. Fig. 10 shows that most of the errors are in a small range. We can find that TSF-CGANs shows a better potential in PV power forecasting.

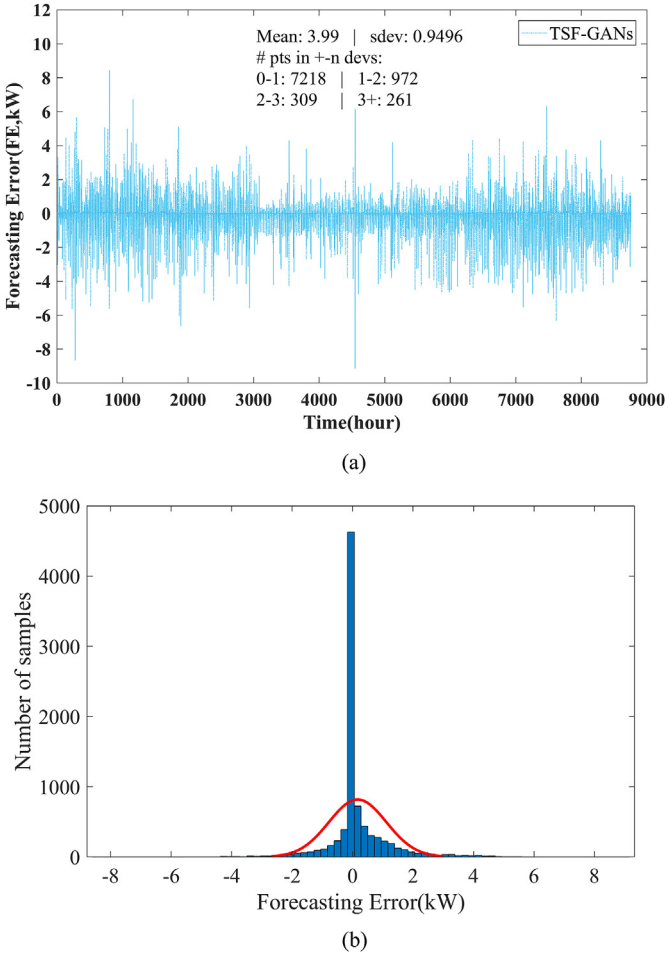

Fig. 10. The forecasting error distribution of test set (Forecasting error, **FE** $= \widehat{\boldsymbol{P}}_{\boldsymbol{i}} - P_{\boldsymbol{i}}$, kW).

3.4. Different algorithms comparison

The calculation results of the proposed TSF-CGAN model and the five comparative models of Persistence, BP, SVM, RNN, and LSTM are shown in Table 2. Simultaneously, the comparison results of RMSE, MAE, and nRMSE are shown in Fig. 11. It can be found that in the comparison of the six models, the proposed TSF-CGANs model has the highest correlation coefficients (R and R^2) and the lowest RMSE and MAE. At the same time, other evaluation indicators also show some advantages. The order of model prediction accuracy is TSF-CGAN, LSTM, the RNN, the SVM, the BP, and the Persistence. The Persistence model does not predict but uses the value at the previous moment as the output at the current moment, so its performance is worst. The persistence model is often used as a benchmark model for comparative research. Compared to the basic BP model (ANN), RNN establishes a connection relationship between the current input and the information of the previously hidden layer, so RNN can capture the dependence between different times and has a better processing capability on time series. The RMSE of the BP, RNN, LSTM, and TSF-CGANs are 1.420, 1.008, 0.993, and 0.964, respectively. Compared with BP, RNN reduced the RMSE by 28.99%, LSTM reduced the RMSE by 30.01%, while the TSF-CGANs model reduced the RMSE by 32.07%. Compared to the RNN-based model, the proposed TSF-CGANs

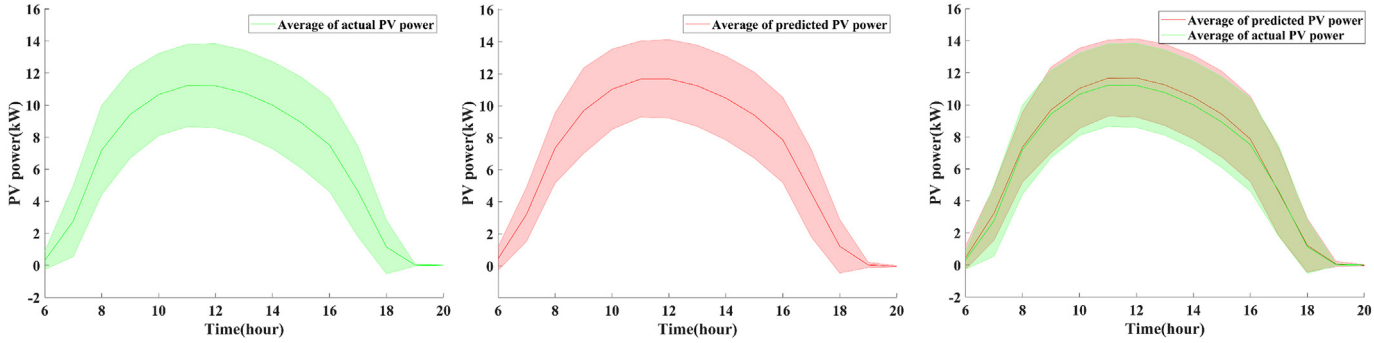

Fig. 9. Statistics of hourly average PV power. Actual PV power (left), predicted PV power (middle) based on TSF-CGANs, and mixed distribution PV power (right).

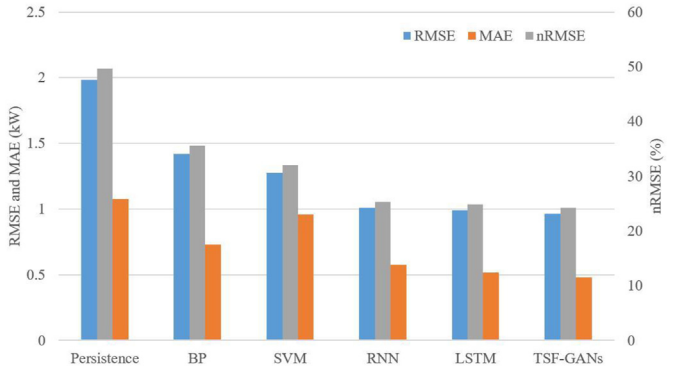

Fig. 11. The RMSE, MAE, and nRMSE of different forecasting models for the test set.

model adds Bi-LSTM and CNN to the generator and discriminator, which takes into account time dependence (through Bi-LSTM) and spatial dependence (through CNN). The performance is further improved by training the adversary architecture.

We randomly selected 5 consecutive days of data from the test sample, and the prediction results of different models are shown in Fig. 12. The red circle and line in the figure represent the true value. It can be seen that the persistence model has an obvious 1-h lag (horizontal ordinate) relative to the true value, which is consistent with the definition of the persistence model. When the true value is 0, the prediction values of the SVM model have a significant deviation. RNN-based models, such as RNN, LSTM, and TSF-CGANs (Note that, both the generator and discriminator in the TSF-CGANs have the Bi-LSTM layer), all have good prediction performance. There are large errors only when the actual value fluctuates violently, and this large fluctuation is a huge challenge for any model. Generally, the prediction result of the TSF-CGANs is very similar to the variation trend of the real PV power data, which confirms that the proposed prediction method has good adaptability and flexibility.

Table 3 displays the monthly RMSE of six models. In April, May, June, July, August, these five months of the year show a small RMSE, especially for the Persistence model. For TSF-CGANs, the RMSE is in the range [0.582 kW–0.840 kW]. In January and February, all models are inaccurate, which may be due to the weather changes in Alice Springs during these periods of the year. At the same time, we also found that the predictions of different models in different months have no obvious similarity, except for the three RNN-based models. The RMSE in different months is different, which may be related to the variations of weather in different months. Therefore, in many studies, the model will be trained and tested by months or seasons.

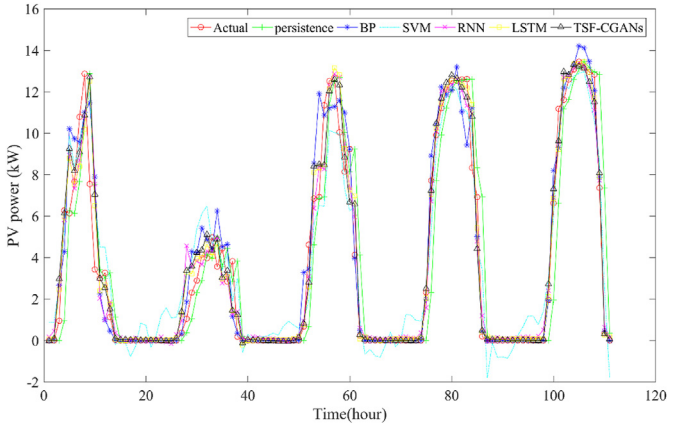

Fig. 12. Results of different models for PV power prediction.

Table 3
The RMSE calculated by different models for each month.

	Persistence	BP	SVM	RNN	LSTM	TSF-CGANs
January	2.193	1.633	1.532	1.289	1.228	1.193
February	2.298	1.510	1.517	1.291	1.249	1.239
March	2.183	1.437	1.353	1.050	1.028	0.972
April	2.137	**1.006**	1.245	0.873	0.843	0.840
May	2.060	1.026	1.255	0.843	0.782	0.769
June	1.849	1.030	1.056	**0.701**	**0.640**	**0.582**
July	1.889	1.117	1.105	0.801	0.779	0.730
August	1.972	1.187	**1.048**	0.800	0.868	0.764
September	1.945	1.313	1.153	0.913	0.978	0.906
October	1.789	1.327	1.327	1.132	1.116	1.088
November	1.707	2.025	1.465	1.234	1.217	1.285
December	**1.688**	1.736	1.160	0.965	0.981	0.950
mean	1.976	1.362	1.268	0.991	0.976	0.943

3.5. Analysis and discussion

Compared with other benchmark models, the proposed method shows slightly better performance in PV power prediction. Although compared to the LSTM model, the performance is only slightly improved, but it still has important significance. This is the first point prediction model of PV power based on the CGANs framework. In the traditional CGANs network, the vast majority of CGANs are used to generate samples with similar distribution features to the actual data. The purpose is to expand the training sample set or increase the generalization ability for the prediction model. In the proposed TSF-CGANs, the generator will generate the next time PV power prediction value using complex CNN, Bi-LSTM, and other networks based on the conditioned matrix and the noise sequence in the latent space. The predicted value or actual value at the next moment, the PV power data at the previous 24 moments, and the conditioned matrix are input to the discriminator, to train and enhance the discriminating ability of the discriminator. Compared with the traditional prediction model, the generator network is more complex and adds noise terms, which can raise the generalization ability of the model, and also prevent vanishing gradient. Meanwhile, the continuous game between the generator and the discriminator improves the prediction accuracy of the generator. This is the biggest contribution and innovation in this paper. Of course, the proposed TSF-CGANs network spends more time on training. But in practical applications, we only focus on the predicted time (testing time), and the training can be completed offline and in free time. In the future, the ongoing research will focus on researching and modifying the discriminator structure to improve its efficiency and calculate prediction errors. We can use the forecasting error instead of true and false judgments to optimize the parameters of the generator and greatly improve the prediction performance.

4. Conclusions

This paper proposed a novel TSF-CGANs model that used the generator of the CGANs network to generate predicted PV power data. Based on the case study, some conclusions can be made as follows.

(1) In the traditional method, the CGANs network is used to directly generate data, and then a mixture of real data and generated data is used to make predictions using predictive

models. Compared with traditional CGANs, this method can directly achieve prediction without other models, which is the first attempt in the time series forecasting field. The advantage of the model is that the uncertainties of PV power were incorporated into the model through reasonably constructing a generator containing a new type of deep neural network, which took into account the noise sequence of the latent space and the conditioned matrix containing multi-dimensional information.

(2) The architecture of the generator and discriminator of the proposed TSF-CGANs model is open and can be configured according to actual applications. In this paper, CNN is used to extract the spatial features of input parameters such as PV power data and GHI data. Bi-LSTM is used to extract temporal features.

(3) The results indicated that the proposed TSF-CGANs can more accurately capture the random distribution and temporal and spatial characteristics of PV power. Compared with the traditional BP forecasting method, the TSF-CGANs model reduced the RMSE by 32%. Compared with the traditional LSTM, the TSF-CGANs model reduced the RMSE by 3%. Compared with Persistence, the forecast skill (FS) of TSF-CGANs is 0.4863.

Although the proposed TSF-CGANs has a very obvious improvement compared with the traditional ANN network, the improvement is not obvious compared with the time series model. The key finding is that CGANs can not only generate training samples but also generate prediction values, which can be directly used for modeling regression models. In the follow-up research, we will focus on discriminator in TSF-CGANs according to the characteristics of the regression problem, so that it can supervise generator can generate more accurate prediction values.

Credit authorship statement

Xiaoqiao Huang: Conceptualization, Methodology, Software, Writing – original draft, Visualization. Qiong Li: Conceptualization, Methodology, Writing – review & editing, Funding acquisition. Yonghang Tai: Methodology, Writing – review & editing. Zaiqing Chen: Conceptualization, Methodology, Writing – review & editing. Jun Liu: Writing – original draft, Visualization. Junsheng Shi: Conceptualization, Review of this paper, Funding acquisition. Wuming Liu: Conceptualization, Review of this paper.

Declaration of competing interest

The authors declare that they have no known competing financial interests or personal relationships that could have appeared to influence the work reported in this paper.

Acknowledgments

This work was supported by the National Natural Science Foundation of China (62062069, 62062070, and 62005235), Natural Science Foundation of Yunnan Province, China (202101AT070100), and Postdoctoral Research Fund of Yunnan Province.

References

[1] IRENA. Renewable capacity statistics 2021. 2021 [https://doi.org/www.irena.org/Publications].
[2] Barbieri F, Rajakaruna S, Ghosh A. Very short-term photovoltaic power forecasting with cloud modeling: a review. Renew Sustain Energy Rev 2017;75:242–63. https://doi.org/10.1016/j.rser.2016.10.068.
[3] Wang H, Yi H, Peng J, Wang G, Liu Y, Jiang H, et al. Deterministic and probabilistic forecasting of photovoltaic power based on deep convolutional neural network. Energy Convers Manag 2017;153:409–22. https://doi.org/10.1016/j.enconman.2017.10.008.
[4] Li P, Zhou K, Lu X, Yang S. A hybrid deep learning model for short-term PV power forecasting. Appl Energy 2020;259:114216. https://doi.org/10.1016/j.apenergy.2019.114216.
[5] Ahmed R, Sreeram V, Mishra Y, Arif MD. A review and evaluation of the state-of-the-art in PV solar power forecasting: techniques and optimization. Renew Sustain Energy Rev 2020;124:109792. https://doi.org/10.1016/j.rser.2020.109792.
[6] Wang H, Liu Y, Zhou B, Li C, Cao G, Voropai N, et al. Taxonomy research of artificial intelligence for deterministic solar power forecasting. Energy Convers Manag 2020;214:112909. https://doi.org/10.1016/j.enconman.2020.112909.
[7] Gr G. Extensive comparison of physical models for photovoltaic power forecasting. Appl Energy 2020:116239. https://doi.org/10.1016/j.apenergy.2020.116239.
[8] Lorenz E, Scheidsteger T, Hurka J, Heinemann Detlev, Kurz C. Regional PV power prediction for improved grid integration. Prog Photovoltaics Res Appl 2011;19:757–71. https://doi.org/10.1002/pip.1033.
[9] Wolff B, Kühnert J, Lorenz E, Kramer O, Heinemann D. Comparing support vector regression for PV power forecasting to a physical modeling approach using measurement , numerical weather prediction. and cloud motion data 2016;135:197–208. https://doi.org/10.1016/j.solener.2016.05.051.
[10] Rafati A, Joorabian M, Mashhour E, Shaker HR. High dimensional very short-term solar power forecasting based on a data-driven heuristic method. Energy 2021;219:119647. https://doi.org/10.1016/j.energy.2020.119647.
[11] Yin H, Ou Z, Zhu Z, Xu X, Fan J, Meng A. A novel asexual-reproduction evolutionary neural network for wind power prediction based on generative adversarial networks. Energy Convers Manag 2021;247:114714. https://doi.org/10.1016/j.enconman.2021.114714.
[12] Wang K, Qi X, Liu H. Photovoltaic power forecasting based LSTM-Convolutional Network. Energy 2019;189:116225. https://doi.org/10.1016/j.energy.2019.116225.
[13] Zhen H, Niu D, Wang K, Shi Y, Ji Z, Xu X. Photovoltaic power forecasting based on GA improved Bi-LSTM in microgrid without meteorological information. Energy 2021;231:120908. https://doi.org/10.1016/j.energy.2021.120908.
[14] Abdel-Basset M, Hawash H, Chakrabortty RK, Ryan M. PV-Net: an innovative deep learning approach for efficient forecasting of short-term photovoltaic energy production. J Clean Prod 2021;303:127037. https://doi.org/10.1016/j.jclepro.2021.127037.
[15] Zhang L, Zhao L. High-quality face image generation using particle swarm optimization-based generative adversarial networks. Future Generat Comput Syst 2021;122:98–104. https://doi.org/10.1016/j.future.2021.03.022.
[16] Wang Z, She QJ, Ward TE. Generative adversarial networks in computer vision: a survey and taxonomy. ACM Comput Surv 2021;54:1–38. https://doi.org/10.1145/3439723.
[17] Beguš G. CiwGAN and fiwGAN : encoding information in acoustic data to model lexical learning with Generative Adversarial Networks. Neural Network 2021;139:305–25. https://doi.org/10.1016/j.neunet.2021.03.017.
[18] Takahashi S, Chen Y, Tanaka-ishii K. Modeling financial time-series with generative adversarial networks. Physica A 2019;527:121261. https://doi.org/10.1016/j.physa.2019.121261.
[19] Wang F, Zhang Z, Liu C, Yu Y, Pang S, Duić N, et al. Generative adversarial networks and convolutional neural networks based weather classification model for day ahead short-term photovoltaic power forecasting. Energy Convers Manag 2019;181:443–62. https://doi.org/10.1016/j.enconman.2018.11.074.
[20] Wei H, Hongxuan Z, Yu D, Yiting W, Ling D, Ming X. Short-term optimal operation of hydro-wind-solar hybrid system with improved generative adversarial networks. Appl Energy 2019;250:389–403. https://doi.org/10.1016/j.apenergy.2019.04.090.
[21] Bendaoud NMM, Farah N, Ben Ahmed S. Comparing Generative Adversarial Networks architectures for electricity demand forecasting. Energy Build 2021;247:111152. https://doi.org/10.1016/j.enbuild.2021.111152.
[22] Chen Y, Wang Y, Kirschen D, Zhang B. Model-free renewable scenario generation using generative adversarial networks. IEEE Trans Power Syst 2018;33:3265–75. https://doi.org/10.1109/TPWRS.2018.2794541.
[23] Zhou B, Duan H, Wu Q, Wang H, Or SW, Chan KW, et al. Short-term prediction of wind power and its ramp events based on semi-supervised generative adversarial network. Int J Electr Power Energy Syst 2021;125. https://doi.org/10.1016/j.ijepes.2020.106411.
[24] Yuan R, Wang B, Mao Z, Watada J. Multi-objective wind power scenario forecasting based on PG-GAN. Energy 2021;226:120379. https://doi.org/10.1016/j.energy.2021.120379.
[25] Zhu B, Jiao J, Tse D. Deconstructing generative adversarial networks. IEEE Trans Inf Theor 2020;66:7155–79. https://doi.org/10.1109/TIT.2020.2983698.
[26] Moon J, Jung S, Park S, Hwang E. Conditional tabular GaN-based two-stage data generation scheme for short-term load forecasting. IEEE Access 2020;8:205327–39. https://doi.org/10.1109/ACCESS.2020.3037063.
[27] Harell A, Jones R, Makonin S, Bajic IV. TraceGAN: synthesizing appliance power signatures using generative adversarial networks. IEEE Trans Smart Grid 2021;12:4553–63. https://doi.org/10.1109/TSG.2021.3078695.
[28] Yin H, Ou Z, Zhu Z, Xu X, Fan J, Meng A. A novel asexual-reproduction

evolutionary neural network for wind power prediction based on generative adversarial networks. Energy Convers Manag 2021;247:114714. https://doi.org/10.1016/j.enconman.2021.114714.
[29] Ahmed R, Sreeram V, Mishra Y, Arif MD. A review and evaluation of the state-of-the-art in PV solar power forecasting: techniques and optimization. Renew Sustain Energy Rev 2020;124:109792. https://doi.org/10.1016/j.rser.2020.109792.
[30] Koochali A, Schichtel P, Dengel A, Ahmed S. Probabilistic forecasting of sensory data with generative adversarial networks - ForGAN. IEEE Access 2019;7:63868–80. https://doi.org/10.1109/ACCESS.2019.2915544.
[31] Goodfellow IJ, Pouget-abadie J, Mirza M, Xu B, Warde-farley D. Generative adversarial nets. Adv Neural Inf Process Syst 2014;27:1–9.
[32] Lan J, Guo Q, Sun H. Demand side data generating based on conditional generative adversarial networks. Energy Proc 2018;152:1188–93. https://doi.org/10.1016/j.egypro.2018.09.157.
[33] Yu H, Chen X, Li Z, Zhang G, Liu P, Yang J, et al. Taxi-based mobility demand formulation and prediction using conditional generative adversarial network-driven learning approaches. IEEE Trans Intell Transport Syst 2019;20:3888–99. https://doi.org/10.1109/TITS.2019.2923964.
[34] Hochreiter S, Schmidhuber J. Long short term memory. Neural Comput 1997;9:1735–80.
[35] Gao M, Li J, Hong F, Long D. Day-ahead power forecasting in a large-scale photovoltaic plant based on weather classification using LSTM. Energy 2019;187:115838. https://doi.org/10.1016/j.energy.2019.07.168.
[36] Srivastava S, Lessmann S. A comparative study of LSTM neural networks in forecasting day-ahead global horizontal irradiance with satellite data. Sol Energy 2018;162:232–47. https://doi.org/10.1016/j.solener.2018.01.005.
[37] Ospina J, Newaz A, Omar Faruque M. Forecasting of PV plant output using hybrid wavelet-based LSTM-DNN structure model. IET Renew Power Gener 2019;13:1087–95. https://doi.org/10.1049/iet-rpg.2018.5779.
[38] Chai M, Xia F, Hao S, Peng D, Cui C, Liu W. PV power prediction based on LSTM with adaptive hyperparameter adjustment. IEEE Access 2019;7:115473–86. https://doi.org/10.1109/ACCESS.2019.2936597.
[39] Zhu F, Ye F, Fu Y, Liu Q, Shen B. Electrocardiogram generation with a bidirectional LSTM-CNN generative adversarial network. Sci Rep 2019;9:1–11. https://doi.org/10.1038/s41598-019-42516-z.
[40] Sharadga H, Hajimirza S, Balog RS. Time series forecasting of solar power generation for large-scale photovoltaic plants. Renew Energy 2020;150:797–807. https://doi.org/10.1016/j.renene.2019.12.131.
[41] Huang X, Li Q, Tai Y, Chen Z, Zhang J, Shi J, et al. Hybrid deep neural model for hourly solar irradiance forecasting. Renew Energy 2021;171:1041–60. https://doi.org/10.1016/j.renene.2021.02.161.
[42] DKASC. Download data, Alice Springs. Desert knowl aust cent. http://dkasolarcentre.com.au/download; 2020.